Journal of Materials Chemistry B

PAPER

Check for updates

A radical containing micellar probe for assessing esterase enzymatic activity with ultra-low field Overhauser-enhanced magnetic resonance imaging†

Sabrina Elkhanoufi,‡[a] Sahar Rakhshan,‡[a] Martin J. Nespeca,[a] Diego Alberti,[a] Dahmane Boudries,[b] Joyce Pokong-Touyam, [b] Rachele Stefania, [c] Elodie Parzy,[b] Philippe Massot,[b] Philippe Mellet, [bd] Jean-Michel Franconi,[d] Eric Thiaudiere*[b] and Simonetta Geninatti Crich [★a]

The ability to track altered enzyme activity using a non-invasive imaging protocol is crucial for the early diagnosis of many diseases but is often challenging. Herein, we show that Overhauser magnetic resonance imaging (OMRI) can be used to monitor enzymatic conversion at an ultra-low field (206 μT) using a highly sensitive ''off/on'' probe with a nitroxide stable radical containing ester, named T2C$_{12}$–T80. This TEMPO derivative containing probe forms stable electron paramagnetic resonance (EPR) silent micelles in water that are hydrolysed by esterases, thus yielding narrow EPR signals whose intensities correlate directly with specific enzymatic activity. The responsiveness of the probe to tumours, facilitated by increased esterase activity, was initially determined by comparing EPR signals measured upon incubation with 3T3 (healthy fibroblasts used as control), HepG2 (human hepatoma) and Hs766T (human pancreatic cancer cells) cell lysates and then with Hs766T and 3T3 living cells. Next, Overhauser MR images were detected on a phantom containing the probe and the esterases to show that the approach is well suited for being translated to the *in vivo* detection at the earth's magnetic field. Regarding detection sensitivity, ultra-low field OMRI (ULF-OMRI) is beneficial over OMRI at higher fields (*e.g.* 0.2 T) since Overhauser enhancements are significantly higher and the technique is safe in terms of the specific absorption rate.

Introduction

Quantitative detection and monitoring of enzymatic activity play a crucial role in diagnostic medicine by enabling a greater understanding of disease processes, early detection and tailored treatment strategies, leading to the development of novel diagnostic and therapeutic tools.[1] Despite its immense diagnostic potential, rapid, sensitive, and high-resolution detection of enzymatic activity *in vivo*, particularly in relatively deep

tissues, remains a significant challenge. Optical imaging modalities that are widely used to assess enzyme activities in cells and animal models are hampered *in vivo* by well-known issues associated with the penetration and scattering of light by animal tissues.[2,3] Analogous PET and SPECT techniques, although endowed with excellent sensitivity, cannot be exploited to monitor chemical transformations in which the radioactive element is the same in the parent and daughter species.[4–6] Alternatively, magnetic resonance imaging (MRI), with or without the involvement of exogenous contrast agents,[7,8] provides the required properties of high resolution and tissue penetration, but its limited detection sensitivity may represent a drawback. Moreover, it often necessitates the use of complex ratiometric protocols as the detection method frequently entails measuring a change in an NMR parameter (T_1, T_2, and CEST response) inherently affected by the concentration of the contrast agent. Therefore, it is evident that there is a need to explore innovative methodologies that are capable of addressing sensitivity and tissue penetration as well as are, ideally, accessible at costs, thus permitting widespread access. Low-field and ultra-low-field MRI

[a] *Department of Molecular Biotechnology and Health Sciences, University of Torino, Via Nizza 52, 10126 Torino, Italy. E-mail: simonetta.geninatti@unito.it*

[b] *Magnetic Resonance Center UMR, Univ. Bordeaux, CNRS, CRMSB, UMR 5536, Case 93 146, rue Leo Saignat, F-33000 Bordeaux, France. E-mail: eric.thiaudiere@rmsb.u-bordeaux.fr*

[c] *Department of Science and Technological Innovation, University of Eastern Piedmont "Amedeo Avogadro", Alessandria, Italy*

[d] *INSERM, Bordeaux, France*

† Electronic supplementary information (ESI) available. See DOI: https://doi.org/10.1039/d4tb00639a

‡ These authors contributed equally.

This journal is © The Royal Society of Chemistry 2024

J. Mater. Chem. B, 2024, **12**, 10923–10933 | **10923**

technologies have recently gained significant interest as an emerging field owing to their unique advantages, such as portability and low cost.[9–12] Although low-field MRI has several advantages, it has certain limitations, including a lower signal-to-noise ratio and reduced spatial resolution compared to high-field MRI. One strategy to increase sensitivity is to use dynamic nuclear polarization (DNP), also known as the Overhauser effect. This technique exploits the dipole–dipole interaction between the electron and the nuclear spin, which, upon saturating the Zeeman states of the unpaired electrons, leads to a polarization transfer to the protons in their proximity that become hyperpolarized.[13–15] In MRI, this approach has often been deemed Overhauser MRI (OMRI). When the catalytic conversion of a radical containing substrate into the reaction product is accompanied by a change in the EPR signal, OMRI can act as a reporter of the ongoing enzymatic activity. Using this diagnostic strategy, the activity of some enzymes, such as proteases,[16,17] elastases,[18] and phospholipases,[19] have been detected *in vitro* and *in vivo* on mice with inflamed lungs[20,21] on a low field MRI system operating at 0.19 T. The main drawback of this approach is the EPR irradiation that occurs at microwave wavelengths (GHz or above), thus generating harmful tissue heating and shallow wave penetration. Therefore, the *in vivo* translation of OMRI to larger animals and humans must imply the use of lower fields (<1 mT). Interestingly, when radical species with hyperfine coupling are employed, it has been demonstrated both theoretically and empirically that the DNP enhancement factor increases as the strength of the static magnetic field decreases.[22,23] This effect can be exploited to partially compensate for the loss of the NMR signal at very low fields, paving the way for molecular imaging studies using OMRI. In this context, the University of Bordeaux developed a home-made earth-field double resonance system capable of producing Overhauser-enhanced MR images in living rats by *in situ* DNP at 206 µT (*i.e.* very close to the earth's magnetic field) using stable and non-toxic nitroxides.[24] Using this system, the protease-driven hydrolysis of a specific nitroxide probe was detected in a preliminary spectroscopy-based approach in which the enzymatic transformation involved a net shift in the EPR frequencies of the parent and daughter species.[25] In this context, we deemed it of interest to design an off/on OMRI agent that can report on a specific enzymatic activity. Recently, our group synthesized esters containing TEMPO derivatives, namely TEMPO-C12 (TC_{12}) and TEMPO-2-C12 ($T2C_{12}$), which formed stable micelles in water, resulting in EPR silence.[26] However, narrow and intense EPR signals are produced following the release of the free TEMPO radicals due to the hydrolysis of the ester bond catalysed by esterases, whose activity is directly correlated with the intensity of the observed EPR signals. Esterases, a subclass of the hydrolase enzyme superfamily, are responsible for hydrolysing ester bonds[27] in various substrates and are involved in the reprogramming of metabolic pathways, promotion of cancer pathogenesis, drug metabolism and drug toxicity.[28,29] Therefore, the detection of esterase activity appears to be a valuable tool for assessing various biological processes, diagnosing and monitoring disease progression and the effect of undertaken therapies.[30–32] Our preliminary results showed that the off/on $T2C_{12}$ probe, upon the hydrolysis of the ester bond, displayed narrow peaks because of the release of small-sized, highly mobile nitroxide radicals in principle suitable for OMRI applications.[26] In the present study, a further improvement of the probe sensitivity has been pursued using a new formulation of $T2C_{12}$ with Tween 80 (T80) that allows the formation of smaller micelles endowed with faster hydrolysis kinetics in the presence of the target enzymes (Fig. 1). By exploiting the DNP effect induced through the radiofrequency saturation of the EPR signal, it was possible to detect, for the first time, a marked enzyme-dependent enhancement in the OMRI image arising from the Overhauser effect at the ultra-low magnetic field strength of 206 µT, *i.e.* at a value close to earth field (25–65 µT). The enhanced signal acts as an efficient reporter of the enzymatic activity, potentially enabling detection in living subjects. Without DNP, the presence of nitroxide would not have been able to generate any enhancement effect in conventional NMR/MRI experiments because only the application of DNP allows an increase in proton polarization in media containing 4-oxo-TEMPO.
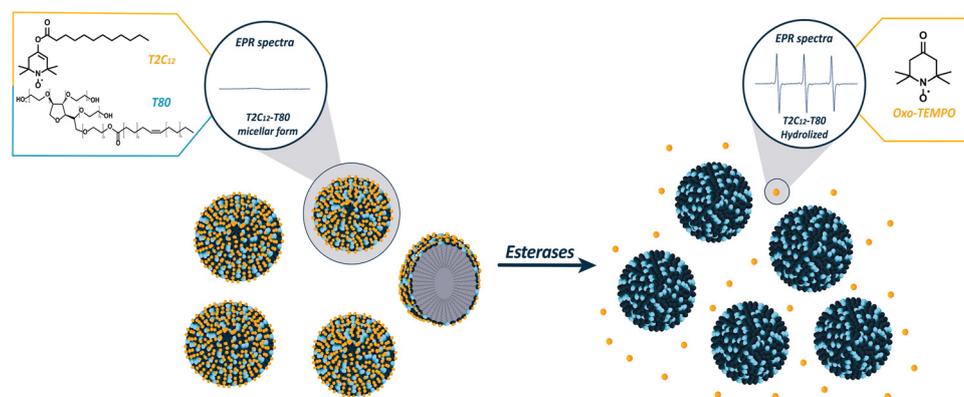

Fig. 1 Schematic representation of the EPR silent $T2C_{12}$–T80 probe in the micellar form, followed by hydrolyzation in the presence of esterases and release of oxo-TEMPO, which display an intense EPR signal.
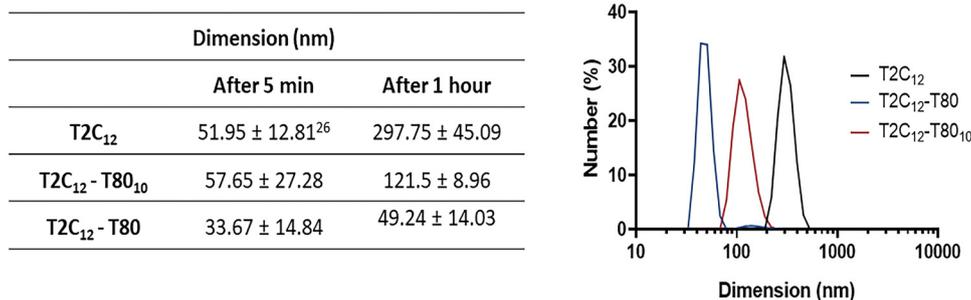
10924 | *J. Mater. Chem. B*, 2024, **12**, 10923–10933

This journal is © The Royal Society of Chemistry 2024

	Dimension (nm)	
	After 5 min	After 1 hour
$T2C_{12}$	51.95 ± 12.81^{26}	297.75 ± 45.09
$T2C_{12} - T80_{10}$	57.65 ± 27.28	121.5 ± 8.96
$T2C_{12} - T80$	33.67 ± 14.84	49.24 ± 14.03

Fig. 2 (left) Table with hydrodynamic diameters of $T2C_{12}$ 100 µM, $T2C_{12}–T80_{10}$ 100 µM and $T2C_{12}–T80$ 100 µM measured *via* DLS 5 min and 1 hour after the sonication step. (right) Number-weighted average size determined for $T2C_{12}$ 100 µM, $T2C_{12}–T80_{10}$ 100 µM and $T2C_{12}–T80$ 100 µM micelles *via* DLS measurement after 1 hour from the sonication step.

Results and discussion

Mixed micelle formulation, characterization, and enzymatic assays

In our previous work,[26] *in vitro* experiments with $T2C_{12}$ micelles and enzymes showed incomplete hydrolysis of the probe. Thus, a novel formulation employing the non-ionic surfactant Tween 80 (T80) was explored to diminish the size of the aggregated nanostructures and boost the performance of the radical containing probe. $T2C_{12}$ mixed micelles were prepared by simply dissolving $T2C_{12}$ in DMSO, then diluting the solution in a HEPES-buffered saline medium containing Tween 80 and sonicating the solution using an ultrasonic homogenizer. Two concentrations of T80, 10 mol% and 20 mol%, were considered. In both cases, the mixture of $T2C_{12}$ and Tween 80 self-assembled into colloidal nanoaggregates characterized by enhanced stability and reduced size.[33] The EPR spectra of both formulations exhibited very low and broad EPR signals identical to those previously observed for the $T2C_{12}$ probe (Fig. S1, ESI†). The micelles made with 20 mol% ($T2C_{12}–T80$) showed greater stability, with hydrodynamic diameters of about 30–40 nm, which remained below 70 nm when measured after 1 hour from the sonication step. Conversely, when the T80 concentration was brought to 10 mol% ($T2C_{12}–T80_{10}$), the mixture resulted in reduced micelle stability, as their hydrodynamic diameter increased to 120 nm after 1 hour from sonication. Notably, the diameter of micelles prepared with only $T2C_{12}$ without T80 was significantly higher (>300 nm) (Fig. 2). Additional characterization with FESEM confirmed the morphology and size of the nanoparticles (Fig. S2, ESI†) and DLS measurements showed neutral zeta potential values with the $T2C_{12}–T80$ and $T2C_{12}–T80_{10}$ (Fig. S3, ESI†). The ability of the micellar radical probes to act as a reporter of the enzymatic activity was initially tested with the porcine liver esterases (PLE), and both formulations with 10 mol% and 20 mol% T80 revealed almost complete hydrolysis ($>90\%$), at a significantly faster rate when compared to the micelles without T80 (Fig. 3). Then, a different class of esterases, namely human carboxylesterases (CEs), was explored. The two major isoforms, carboxylesterases 1 (CEs1) and carboxylesterases 2 (CEs2),[34] are highly expressed under many pathologic conditions.[35,36] As found in our previous study with $T2C_{12}$,[26] the mixed micelles displayed a much higher efficiency with CEs2 than CEs1, demonstrating a nearly complete
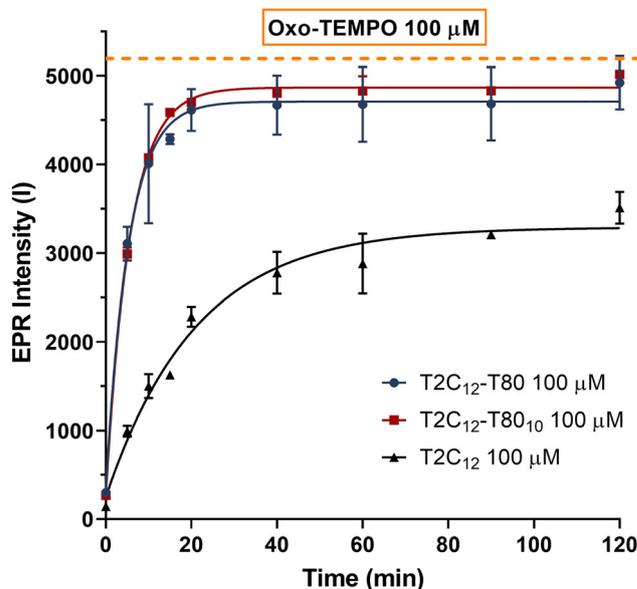

Fig. 3 EPR enzymatic assays with 0.5 U mL^{-1} of PLE in the presence of $T2C_{12}$ 100 µM, $T2C_{12}–T80_{10}$ 100 µM or $T2C_{12}–T80$ 100 µM micelles maintained at 37 °C under stirring at 400 rpm. The continuous line is drawn to better show the course of the points.

and faster hydrolysis of $T2C_{12}$, which confirms the superiority of the new formulation (Fig. 4).

Micelle stability

The mixed micelles stability was evaluated in human serum (HS) and a buffered solution of human serum albumin (HSA). Fig. 5 shows that a similar hydrolytic behaviour occurred in serum and HSA containing medium, where the protein is at the same concentration found in serum (40 mg mL^{-1}). Thus, the modest hydrolysis observed in HS is likely due to the slight esterolytic activity of HSA as reported by Ascenzi *et al.*[37–39] Even though the physiological significance of HSA esterolytic activity and its natural substrates remain unclear, HSA can hydrolyse various compounds, including[40] long- and short-chain fatty acid esters, potentially influencing various pharmacokinetic or toxicokinetic processes.[38] The T80-containing mixed micelles
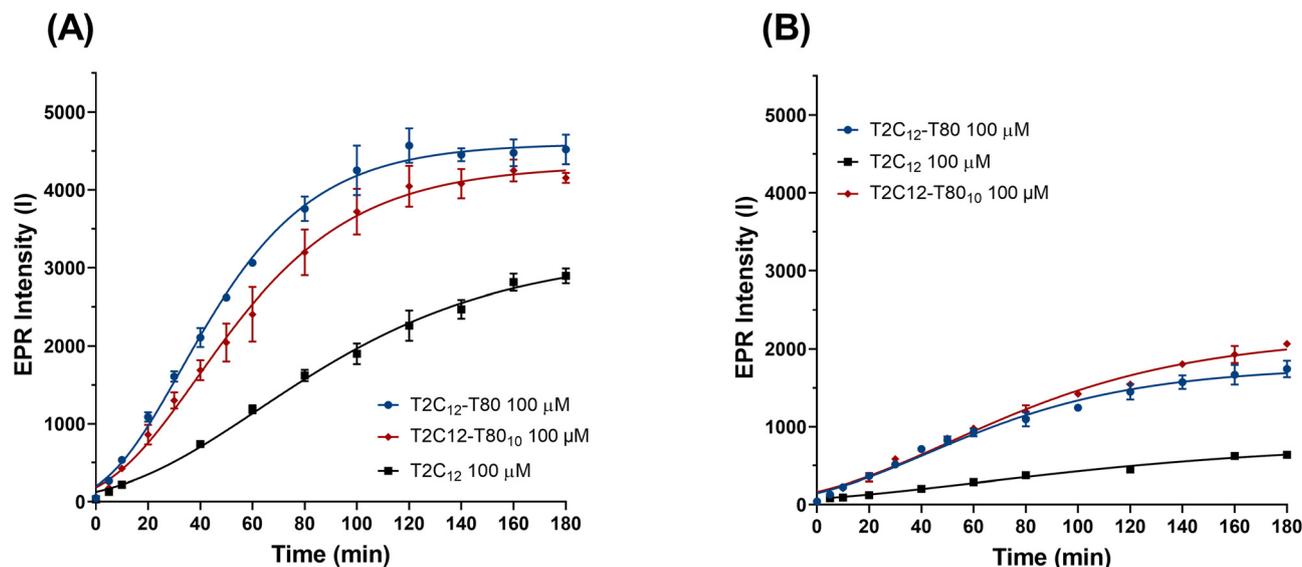
This journal is © The Royal Society of Chemistry 2024

J. Mater. Chem. B, 2024, **12**, 10923–10933 | **10925**

Fig. 4 (A) EPR enzymatic assays with 12 U mL^{-1} of CEs2 in the presence of T2C$_{12}$ 100 μM, T2C$_{12}$–T80$_{10}$ 100 μM and T2C$_{12}$–T80 100 μM. (B) Enzymatic assays of T2C$_{12}$ 100 μM, T2C$_{12}$–T80$_{10}$ 100 μM and T2C$_{12}$–T80 100 μM with CEs1 12 U mL^{-1}. All kinetics were performed at 37 °C with stirring at 400 rpm, and the continuous line was drawn to better show the course of the points.

showed a significantly faster hydrolysis rate in serum compared to T2C$_{12}$ alone. Despite the reduced stability of the micelles in

Fig. 5 (A) Incubation of T2C$_{12}$ 100 μM, T2C$_{12}$–T80$_{10}$ 100 μM and T2C$_{12}$–T80 100 μM with human serum. (B) Incubation of T2C$_{12}$ 100 μM, T2C$_{12}$–T80$_{10}$ 100 μM and T2C$_{12}$–T80 100 μM with HAS containing medium 40 mg mL^{-1}. The assays were performed at 37 °C under stirring at 400 rpm and measured after 3 min, 1 h and 2 h of incubation. The results are reported as a percentage of hydrolyzation (% hydrolyzation) that was calculated using a calibration curve of 4-oxo-TEMPO (Fig. S4, ESI†).

serum, due to the addition of T80, the hydrolysis kinetics remained remarkably faster in the presence of specific esterases (Fig. 6). After 1 h of incubation, T2C$_{12}$–T80 in the presence of PLE and CEs2 produced a much higher EPR signal compared to the ones observed in human serum alone (Fig. 6). Therefore, the formulation with 20 mol% of T80 (T2C$_{12}$–T80), due to its smaller size and slightly improved stability in HS and HSA-containing solutions, was selected for the following *in vitro* experiments.

Because biological systems require a reducing environment to maintain the redox status of living cells, we examined the resistance to the reduction of the nitroxide radicals within the micelles. This evaluation occurred in the presence of ascorbic acid (AC), which is an abundant molecule in the bloodstream.[41] As already reported, nitroxide radicals are generally not stable in a reducing environment.[42,43] In fact, with AC 1 mM, a complete reduction of the parent 4-oxo-TEMPO to the
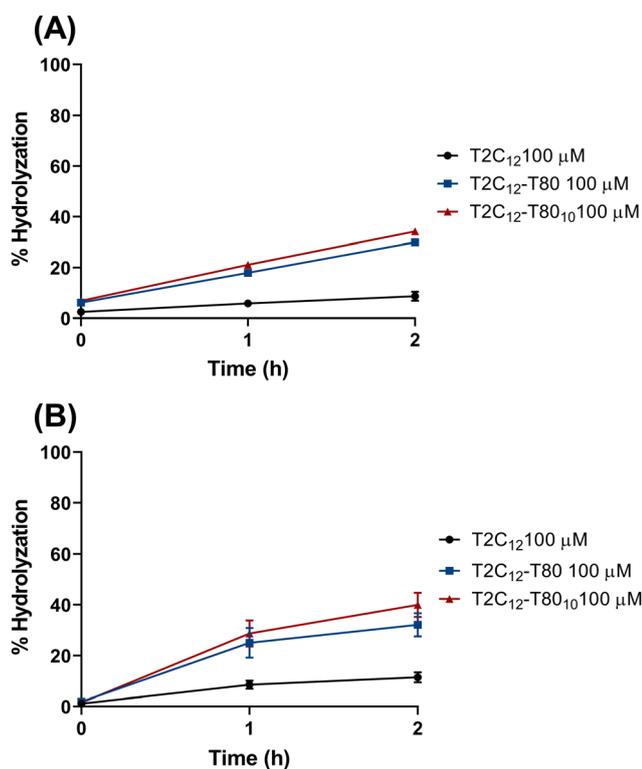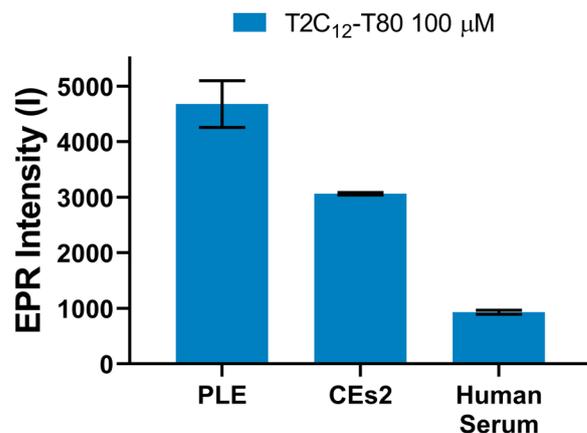

Fig. 6 EPR intensity detected upon 1 h incubation of T2C$_{12}$ 100 μM + T80 20 μM with PLE, CEs2 and human serum at 37 °C under stirring at 400 rpm.

10926 | *J. Mater. Chem. B*, 2024, **12**, 10923–10933

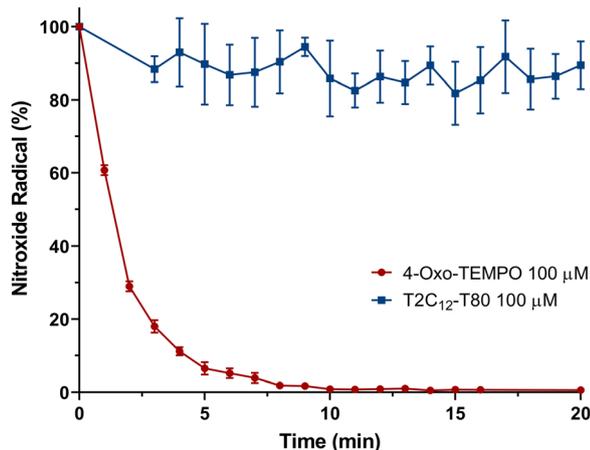This journal is © The Royal Society of Chemistry 2024

Fig. 7 Residual nitroxide radical (%) of 4-oxo-TEMPO 100 μM (red) and T2C$_{12}$–T80 100 μM (blue) in the presence of ascorbic acid 1 mM at room temperature for 20 min.

respective EPR silent hydroxylamine was observed in only few min. (Fig. 7). Interestingly, T2C$_{12}$–T80 micelles exhibited significantly enhanced radical stability when incubated with AC 1 mM, with only an $11 \pm 6\%$ and 60% reduction in the EPR signal after 20 minutes and 2 hours (Fig. S5, ESI†), respectively. The stability was also investigated at higher micelle concentrations (2 mM), which was used in the below OMRI experiments. In the presence of human serum (Fig. 8A), minor hydrolyzation
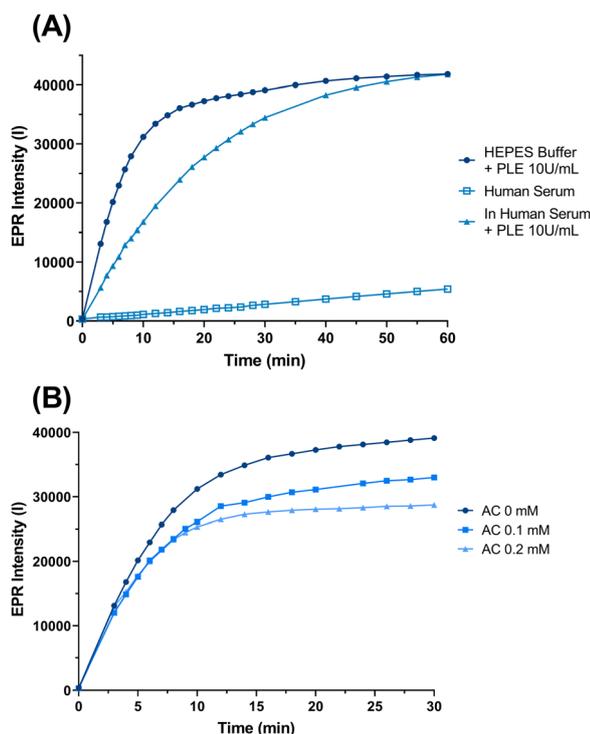

Fig. 8 Stability assessment with T2C$_{12}$–T80 2 mM. (A) Incubation of the micelle probe HS and enzymatic kinetics with PLE 10 U mL^{-1} in HEPES-buffered saline solution or in human serum. (B) Enzymatic kinetics with PLE 10 U mL^{-1} in the absence and presence of ascorbic acid of 0.1 and 0.2 mM. All the assays were performed at room temperature.

of the probe (12% compared to PLE) was observed after 1 hour of incubation. However, a slower but complete kinetic was detected in the presence of PLE, confirming the ability of the probe to assess the esterase activity despite slight hydrolyzation by the serum. Although in the presence of 0.1 mM and 0.2 mM of AC (Fig. 8B), corresponding to the endogenous concentrations present in plasma and tissue, respectively,[44] only a 16% reduction in the free radical released following the hydrolyzation was noted. This observation underscores the remarkable stability of radicals when encapsulated within micelles, even in the presence of reducing agents, underlining a clear advantage for their utilization in *in vivo* studies.

In vitro esterase assessment

To evaluate the expression of esterases under different pathologic conditions, preliminary tests were performed using cytosolic cell extracts of the human pancreatic cancer (Hs766T), human hepatocarcinoma (HepG2) and fibroblast (3T3) cell lines. Hs766T and HepG2[45–48] were chosen as tumour models due to the significantly higher levels of cytosolic esterases compared to healthy cells, represented in this study by 3T3 fibroblast cells.[49,50] To validate the reported higher levels of cytosolic esterases in cancer cells compared to healthy cells, a fluorometric assay based on fluorescein diacetate (FDA) was employed. FDA is an esterified fluorogenic substrate widely used for assessing esterase activity in bacteria.[51,52] It permeates cells by undergoing hydrolysis of its diacetate (DA) groups into fluorescent fluorescein by intracellular nonspecific esterases. As depicted in Fig. 9, consistent with the literature findings, both tumour cell lines (Hs766T and HepG2) exhibit significantly elevated esterase concentrations in their cytosolic extracts compared to healthy 3T3 cells. Moreover, FDA hydrolysis exhibits relatively rapid kinetics, allowing for differentiation between different cell lines within an hour. Similarly, the incubation of the T2C$_{12}$–T80 probe with the cytosolic cell extracts showed a significant increase in the EPR signal with
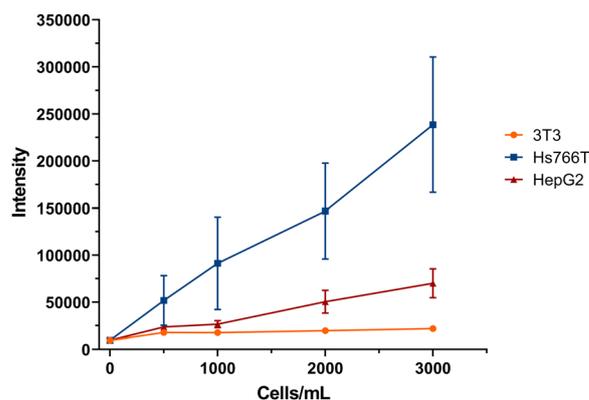

Fig. 9 Fluorescence-detected enzymatic assay, achieved after 1 hour of incubation at 37 °C with stirring at 400 rpm with samples containing FDA 30 nM and 3T3, Hs766T and HepG2 cell lysate. Cells per mL indicate the number of cells used to obtain cell lysates and incubated with FDA before dilution for fluorescence measurements.
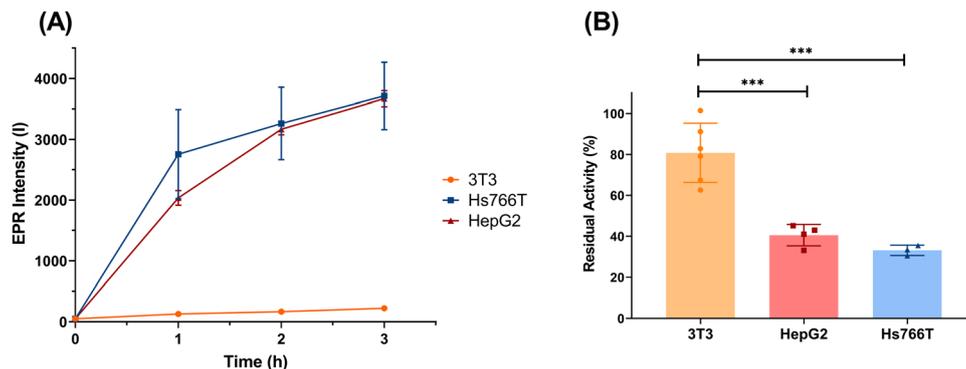
This journal is © The Royal Society of Chemistry 2024

J. Mater. Chem. B, 2024, **12**, 10923–10933 | **10927**

Fig. 10 EPR assay of carboxylesterase enzymatic activity. (A) Incubation of T2C$_{12}$–T80 100 μM with cytosolic extracts of 3T3, Hs766T, and HepG2 cells, each obtained from 250 × 10^3 cells at 37 °C under stirring at 400 rpm for 3 hours. (B) Residual activity measured after 3 hours of incubation in the presence of the carboxylesterase inhibitor (BNPP 600 μM); 100% correspond to the values obtained in the absence of the inhibitor. Statistical significance was determined using an unpaired student's t-test calculated with GraphPad prism version 8.0.2 ($P > 0.05$ is ns, $P \leq 0.05$ is *, $P \leq 0.01$ is **, $P \leq 0.001$ is ***, and $P \leq 0.0001$ is ****).

cytosolic extracts of tumour cells (Hs766T and HepG2) (Fig. S6, ESI†), whereas no change was detected with the cytosolic extracts of healthy cells (3T3 fibroblasts) (Fig. 10A). The observed increase corresponds to the hydrolysis of approximately 70% of the radical containing species as the result of the esterase activity in the cytoplasmatic extracts. More insights into the specificity of the T2C$_{12}$–T80 radical probe were gained by repeating the experiment in the presence of an excess of bis-nitrophenylphosphate (BNPP),[34] a specific inhibitor of carboxylesterases (Fig. S7, ESI†). In the case of the two tumour cell lines, a remarkable decrease in the intensity, with residual activity around 30–40%, was observed, while only a 20% reduction was recorded in the case of healthy 3T3 (Fig. 10B). Following the promising results obtained by comparing cell lysates, specifically by Hs766T and 3T3, the response of the T2C$_{12}$–T80 incubated in the presence of intact living cells was investigated (Fig. 11). The obtained results showed a significant difference (P value ≤ 0.001) in the EPR intensity between the tumour (Hs766T) and healthy (3T3) cell lines after 30 min of incubation of T2C$_{12}$–T80 in the cell culture medium. This trend continued even after 1 hour of incubation, with a P-value of ≤ 0.0001. The normalized EPR intensity with the number of cells present on the dishes still revealed a significant difference (P value ≤ 0.001) between the two cell lines. Therefore, the high EPR signal observed in the experiment with the pancreatic tumour cells confirmed the upregulation of the hydrolytic enzymes accessible to the probe (T2C$_{12}$–T80). These observations do not provide information on the enzyme location, specifically whether they are found on the cell membrane or released into the extracellular medium.[53–55] Uptake assays were carried out using T2C$_{12}$–T80 and 4-oxo-TEMPO on Hs766T cells. In both cases, after 24 hours of incubation, no EPR signal was detected in the cell pellets (Fig. S8, ESI†), which indicates a fast reaction with ROS present in the intracellular environment. The toxicity of T2C$_{12}$–T80 and T2C$_{12}$ micelles was evaluated against Hs766T and 3T3 cell lines using an MTT assay to ensure that, within the concentration range used to assess esterase activity, there was no observed toxicity, and that the compounds were
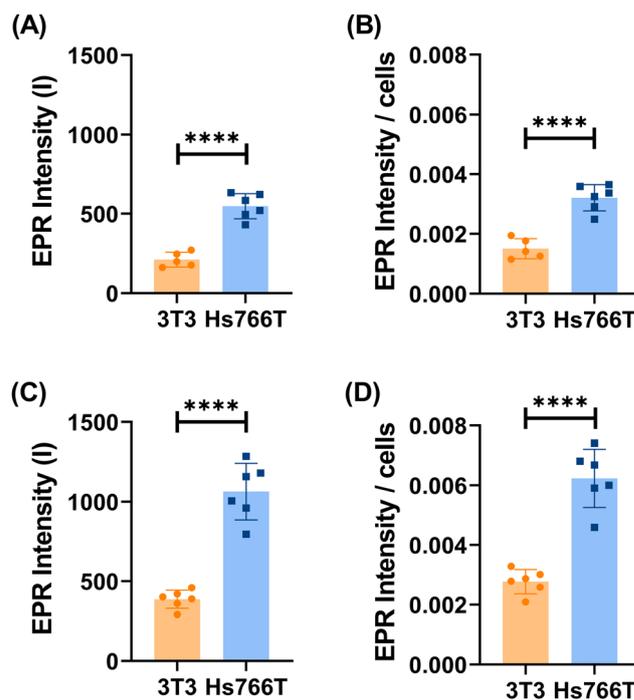

Fig. 11 *In vitro* assessment of esterase activity with 3T3 and Hs766T cells with T2C$_{12}$–T80 100 μM at 37 °C. Absolute EPR intensities (A) and their values normalized to the number of cells (B) after 30 and after 1 hour (C) and (D) of incubation. Statistical significance was determined *via* an unpaired student's t-test calculated with GraphPad prism version 8.0.2 ($P > 0.05$ is ns, $P \leq 0.05$ is *, $P \leq 0.01$ is **, $P \leq 0.001$ is ***, and $P \leq 0.0001$ is ****).

biosafe within the concentration range investigated (< 300 μM) (Fig. S9, ESI†). The excellent sensitivity, biocompatibility and stability exhibited by T2C$_{12}$–T80 micelles make them a highly suitable option for serving as a specialized sensor for assessing the enzymatic activity in the first OMRI experiment at ultra-low magnetic strengths.
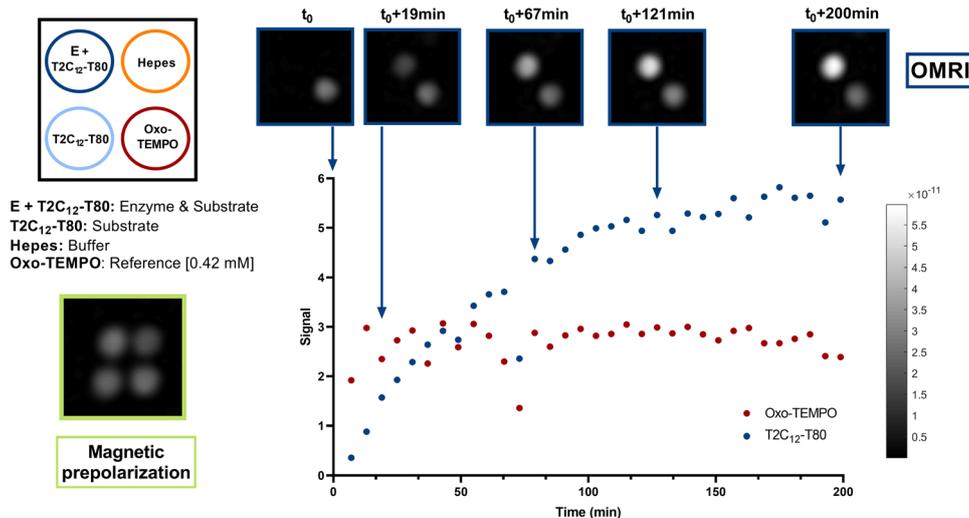
10928 | *J. Mater. Chem. B*, 2024, **12**, 10923–10933

This journal is © The Royal Society of Chemistry 2024

Fig. 12 OMRI monitoring of the enzymatic reaction between T2C$_{12}$–T80 2 mM and PLE 1 U mL^{-1} for 200 minutes at room temperature. The phantom contained the following 4 sample tubes: (blue) T2C$_{12}$–T80 2 mM with PLE 1 U mL^{-1}, (orange) HEPES-buffered saline solution, (red) 4-oxo-TEMPO at 0.42 mM in HEPES-buffered saline solution and (light blue) T2C$_{12}$–T80 2 mM in HEPES-buffered saline solution. Comparison with the MR image obtained for the phantom upon the application of Zeeman pre-polarization at 20 mT is also shown (green border).

Assessment of the esterase activity by OMRI at ultra-low field

Based on the above-reported results, an OMRI experiment was performed at an ultra-low field of 206 μT to monitor the enzymatic kinetics with T2C$_{12}$–T80 and PLE. The experiment was executed with a phantom containing four sample tubes made of three controls (HEPES-buffered saline solution, 4-oxo-TEMPO at 0.4 mM and T2C$_{12}$–T80 2 mM) and one with T2C$_{12}$–T80 2 mM and PLE 1 U mL^{-1}. The spatial distribution of the samples in the phantom could be clearly delineated in conventional MR spin-echo images after Zeeman pre-polarization at 20 mT, *i.e.* at a field that is two orders of magnitude higher than that used in the OMRI experiment. This step was mandatory in the absence of DNP because no measurable NMR signal would have been observed with the experimental magnetic spin polarization achievable at 206 μT. The OMRI kinetics of enzymatic hydrolysis were measured at room temperature and followed for 200 min with the acquisition of a new image every 6 minutes. The results reported in Fig. 12 demonstrate that the signals arising from the 4-oxo-TEMPO reference solution and the enzyme-free T2C$_{12}$–T80 micelles solution remained fairly constant over time, with a complete "quenched" signal in the case of the micelles. Conversely, the OMRI signal increased over time in the enzyme containing solution. The reaction appeared complete after 200 minutes and the concentration of the radical in the OMRI-reference and in the enzyme containing sample, as measured by EPR, yielded values of 0.42 mM and 1.35 mM, respectively. During the OMRI experiment, the sample temperature showed a small increase, from 27 °C to 31 °C, due to RF deposition (15 W EPR continuous wave irradiation; 30 s duration at the frequency of 71.6 MHz). This temperature variation does not significantly affect the reaction kinetics, thus maintaining the validity of the proposed method. The obtained results clearly demonstrate the ability of the ultra-low field

OMRI instrument to detect and measure *in vitro* the contrast built up from the enzyme activity on a properly designed off/on responsive agent. Notably, as depicted in Fig. 12, one can estimate that T2C$_{12}$ concentration as low as 0.2 mM, corresponding grossly to time-point t_0 + 19 minutes, is sufficient for generating enough contrast in 2D-OMRI in half a minute imaging time. An analogous sensitivity was observed in the previously published *in vitro* experiments.[24] This low concentration of a non-toxic nitroxide appears compatible with values encountered in *in vivo* experiments in rodents with no significant adverse effects.[20,21,24]

Conclusions

In our previous paper,[26] we reported on the synthesis and characterization of a TEMPO-based radical functionalized with an aliphatic chain (T2C$_{12}$) through the insertion of an ester bond that can be easily hydrolysed by esterases. The T2C$_{12}$ forms in water EPR silent micelles that can be activated by the enzymes. Following the release of the free TEMPO radicals, narrow and intense EPR signals are produced due to the hydrolysis of the ester bond catalysed by esterases whose activity is directly correlated with the intensity of the observed EPR signals. The results reported in this study showed that the novel formulation of the nitroxide radical T2C$_{12}$ using the non-ionic surfactant Tween 80 (T80) exhibited a higher sensitivity and selectivity to detect esterase activity *in vitro* and in the presence of tumour cells (HepG2 and Hs766T) characterized by esterase overexpression. Interestingly, the resistance to the reduction in the nitroxide radicals forming the micelles was significantly improved with respect to the free oxo-tempo radical, and the "off–on" transition made the methodology semi-quantitative, avoiding the use of complex ratiometric

This journal is © The Royal Society of Chemistry 2024

J. Mater. Chem. B, 2024, **12**, 10923–10933 | **10929**

corrections to eliminate the contribution arising from the nonhydrolyzed probes. Moreover, it was shown that OMRI *in vitro* could serve in the follow-up of an enzymatic conversion at an ultra-low field. As observed from our previous study,[24] the bio-distribution of a conventional nitroxide was measured in living rats in 3D with the same OMRI system within a few minutes of imaging time. In both studies, significant signal enhancement due to DNP could be observed with very limited amounts of nitroxides, *i.e.* for concentrations lower than 0.5 mM. In this context, the indications gained in this work will provide useful insights for the design of further improved responsive agents. Actually, one may envisage additional designs for reporting on the activity of degradation enzymes, such as matrix metalloproteinases (MMPs) and plasminogen activators, in the tumor ECM. Regarding detection sensitivity, ULF-OMRI is beneficial over OMRI at higher fields (*e.g.* 0.2 T)[19,20] because Overhauser enhancements are much lower in the latter case. Moreover, ULF-OMRI is safe in terms of specific absorption rate and allows investigation in large animals. Therefore, a consistent continuation of the present work is the investigation of the fate of the proposed micellar contrast agent *in vivo* in healthy rodents but also in the context of molecular imaging of disease-associated carboxylesterase activity in rodents.

Experimental section

Materials and methods

All the compounds were purchased from Sigma-Aldrich, and all the solvents from VWR. EPR spectra were acquired using the Adani EPR spectrometer Spinscan X (9.2–9.55 GHz) with the following parameters: center field = 336.50 mT, sweep width = 8 mT, sweep time = 30 s, modulation amplitude = 150 µT, and attenuation = 20 dB. All the enzymatic incubations were done in Starlab Thermomixer-Mixer HC at 37 °C under stirring at 400 rpm. The ultrasonic homogeniser Sonicator Bandelin Sonoplus HD 2070 with an M72 tip was used for the sonication of the micelles. The hydrodynamic mean diameter was determined using a Malvern dynamic light-scattering spectrophotometer (Malvern Instruments, Malvern, UK). A fluorescence assay was performed using the spectrofluorometer (Fluoro-Max-4, Horiba Jobin Yvon). Cell lines were purchased from ATCC, while cell culture medium and supplements (foetal bovine serum FBS, glutamine, glucose) were purchased from Euroclone. All the measurements were repeated at least three times, and the results are shown as mean ± standard deviation.

Micelle preparation

T2C$_{12}$ was prepared according to the previously reported procedure, as illustrated by Elkhanoufi *et al.*, 2022.[26] T2C$_{12}$ micelles were obtained by dissolving the nitroxide radical derivative in dimethyl sulfoxide (DMSO) to a final concentration of 33.3 mM. Then, 9 µL of T2C$_{12}$ 33.3 mM was diluted in 991 µL of HEPES-buffered saline solution at pH 7.4 to obtain T2C$_{12}$ 300 µM in micellar form. The solution was then

sonicated for 2 min at 15% power using an ultrasonic homogenizer in an ice bath and diluted to 100 µM in HEPES-buffered saline solution (with a final DMSO concentration of 0.3%). The mixed micelles were obtained using the same procedure by diluting 9 µL of T2C$_{12}$ 33.3 mM in 984 µL HEPES-buffered saline and 7.4 µL of Tween 80 8.12 mM to obtain T2C$_{12}$ 300 µM + T80 60 µM (T2C$_{12}$–T80 300 µM), or 987 µL of HEPES-buffered saline and 3.7 µL of Tween 80 8.12 mM for the T2C$_{12}$ 300 µM + T80 30 µM (T2C$_{12}$–T80$_{10}$ 300 µM, respectively). Similarly, the samples were sonicated for 2 min at 15% power and then diluted to 1 : 3 to achieve T2C$_{12}$ 100 µM + T80 20 µM (T2C$_{12}$–T80 100 µM) or T2C$_{12}$ 100 µM + T80 10 µM (T2C$_{12}$–T80$_{10}$ 100 µM).

DLS measurements

All samples (T2C$_{12}$ 300 µM, T2C$_{12}$–T80$_{10}$ 300 µM and T2C$_{12}$–T80 300 µM) were diluted in the ratio of 1 : 3 in HEPES-buffered saline solution (pH 7.4) after the sonication, freshly filtered (cut-off = 0.2 µm), and measured *via* DLS at 25 °C immediately after dilution and after 1 hour.

Enzymatic kinetic assays

Enzyme kinetic assays were performed using final concentrations of T2C$_{12}$, T2C$_{12}$–T80 or T2C$_{12}$–T80$_{10}$ 100 µM and of CEs2 12 U mL^{-1}, CEs1 12 U mL^{-1} or PLE 0.5 U mL^{-1}, corresponding to concentrations of 23 µg mL^{-1}, 7 µg mL^{-1} and 5 µg mL^{-1}, respectively. All the experiments were carried out at 37 °C under stirring at 400 rpm, and at different intervals, a small sample was taken from the solutions for EPR measurement.

Stability in albumin and serum

The stability of the radicals was evaluated in the presence of human serum albumin (HSA) by adding 10 mg of the protein to 250 µL of T2C$_{12}$, T2C$_{12}$–T80 or T2C$_{12}$–T80$_{10}$ 100 µM to achieve a final HSA concentration of 40 mg mL^{-1}. The serum stability was evaluated using lyophilised human serum (seronorm human) resuspended with 200 µL of 100 µM micelles solutions (T2C$_{12}$, T2C$_{12}$–T80 and T2C$_{12}$–T80$_{10}$). All the experiments were carried out at 37 °C under stirring at 400 rpm, and at different intervals, a small volume was taken from the solutions for EPR measurements.

Stability of ascorbic acid

Ascorbic acid solution was prepared by dissolving 26.8 mg of ascorbic acid (AC) in 1.9 mL of HEPES-buffered saline solution and 150 µL of NaOH 1 M to obtain a solution of AC 74 mM at pH 7.4. The stability assessment of the radicals was performed by incubating 50 µL of oxo-TEMPO 200 µM with 47.3 µL of buffered HEPES saline solution and 2.7 µL of AC 37 mM. Moreover, with the micelles, 50 µL of T2C$_{12}$–T80 300 µM were mixed with 96 µL of HEPES-buffered saline solution and 4 µL of AC 37 mM. At different intervals, a small sample was taken from the solutions for EPR measurement after the addition of AC.

Cell lines

Hs766T, human pancreatic cancer cell line, Hep-G2, human hepatocellular carcinoma cell line and NIH/3T3 (3T3), mouse

10930 | *J. Mater. Chem. B*, 2024, **12**, 10923–10933

This journal is © The Royal Society of Chemistry 2024

embryo fibroblast, were obtained from ATCC. The Hs766T were cultured in Dulbecco's modified Eagle's medium supplemented with 10% (v/v) Fetal bovine serum (FBS), and 2.5 mM of L-glutamine (Lonza). The Hep-G2 cells were cultured in Eagle's minimum essential medium containing 2.5 mM glutamine and EBSS and supplemented with 10% (v/v) FBS and 1 mM sodium pyruvate. The 3T3 cells were cultured in Dulbecco's modified Eagle's medium containing 2.5 mM glutamine and supplemented with 10% (v/v) FBS. All media contained 100 U mL^{-1} penicillin and 100 U mL^{-1} streptomycin. All the cell lines were maintained at 37 °C in a 5% CO_2 incubator.

Cell lysate experiments

Hs766T, HepG2, and 3T3 cells were seeded in 175 cm diameter flasks at the following densities: 1×10^6, 5×10^5, and 3×10^5 cells, respectively. Following an incubation period of nearly 72 hours at 37 °C with 5% CO_2 in a cell incubator, when the confluence reached approximately 70–80%, the cells were washed three times with 10 mL of ice-cold PBS and subsequently detached using a solution containing 0.05% trypsin and 0.02% EDTA. After detachment, all the cell samples were transferred to Falcon tubes and resuspended in 600 μL of PBS, and the cell samples in each condition were counted using trypan blue (Sigma). The cells were then sonicated at 30% power for 1 minute on ice. Subsequently, aliquots of cells with concentrations of 0.5×10^3, 1×10^3, 2×10^3, and 3×10^3 cells per mL were prepared for the fluorimetry experiment, and aliquots containing 250×10^3 cells were prepared for the EPR experiment.

Fluorimetry with cell lysate

Fluorescein diacetate (FDA) solution was dissolved in DMSO to a final concentration of 333 mM. Then, 3 μL of the solution was diluted with 997 μL of HEPES-buffered saline solution to obtain FDA 1 μM. Afterwards, 100 μL of FDA 1 μM was incubated for 60 min at 37 °C and stirred at 400 rpm with a small aliquot of cell lysate (3T3, Hs766T, HepG2), corresponding to 0.5×10^3, 1×10^3, 2×10^3, and 3×10^3 cells per mL. After the incubation, 90 μL was taken from the samples, diluted with 2.91 mL of HEPES-buffered saline solution (FDA/fluorescein final concentration of 30 nM) and measured using the fluorescence spectrometer. The excitation and emission parameters were set at 490 nm and 510 nm, respectively.

EPR with cell lysate

The experiment was carried out by adding 100 μL of T2C$_{12}$–T80 300 μM to a volume of cell lysate corresponding to 250×10^3 cells and diluted with HEPES-buffered saline solution to a final volume of 300 μL. The samples were then incubated at 37 °C and 400 rpm, and after 1, 2 and 3 hours, a small aliquot was taken for the EPR measurement. The inhibition experiment was performed using bis(4-nitrophenyl)phosphate (BNPP). After solubilizing the inhibitor in HEPES-buffered saline solution to a final concentration of 5.4 mM, the pH was corrected to 7.4 and sonicated in an ultrasonication bath at 30 °C for 30 minutes. To inhibit the enzyme activity, preincubation was

done by adding 16 μL of BNPP 5.4 mM to the cell lysate solution and HEPES-buffered saline solution at 37 °C and 400 rpm for 30 min. Then, 100 μL of micelle solution was added to obtain a solution with T2C$_{12}$–T80 100 μM with BNPP 600 μM and 250×10^3 cell lysate (final volume of 300 μL).

EPR with living cells

Hs766T and 3T3 cells were seeded in 3 cm dishes at 10×10^4 and 20×10^4 densities for 3T3 and Hs766T, respectively. After 24 h of incubation, the medium was replaced with a serum-free medium, and after 30 min, the cells were incubated with 100 μM T2C$_{12}$–T80 in a final volume of 1 mL at 37 °C for 30 and 60 min, respectively. At these time intervals, 60 μL of the medium was collected and analysed using EPR. The cells were then washed once with 0.5 mL of ice-cold PBS and detached using a solution of 0.05% trypsin and 0.02% EDTA. The cell samples in each condition were counted using trypan blue.

MTT

In a 96-well microtiter plate, 11×10^4 and 6.5×10^3 cells per well were seeded for the Hs766T and NIH/3T3 cell lines, respectively. Following a 24-hour incubation period at 37 °C and 5% CO_2, the cells were subjected to escalating concentrations of T2C$_{12}$–T80 and T2C$_{12}$ (ranging from 0 to 300 μM) and further incubated for an additional 24 hours under normoxic conditions (at 37 °C and 5% CO_2). The concentration of dimethyl sulfoxide (DMSO) in the cell medium did not surpass 0.3% (v/v) under all tested conditions. After the incubation period, the medium was aspirated, and each well was treated with thiazolyl blue tetrazolium bromide (Sigma Aldrich) dissolved in the medium at a concentration of 0.45 mg mL^{-1}. The cells were then incubated for 4 hours at 37 °C and 5% CO_2. Subsequently, the medium was removed, and 150 μL of DMSO was added to each well to dissolve the formazan salt crystals produced due to live cell metabolism. The microplate was incubated at room temperature for 30 minutes, after which the absorbance was measured at 565 nm using the GloMax® Discover Microplate Reader (Promega Corporation, Milano, Italy). Cell viability was assessed as the percentage of dead cells observed in the treated samples relative to the non-treated control cells.

OMRI experiments

Ultra-low field Overhauser-enhanced magnetic resonance imaging was performed using a system already described (Boudries *et al.*, 2023).[24] Briefly, the system is composed of concentric cylinder-shaped elements: a gradient coil (280 mm diameter), a Zeeman prepolarization coil allowing 20 mT B_0-field (150 mm diameter), an NMR coil operating at 8.77 kHz (second-order solenoid gradiometer, 80 mm diameter) and an EPR coil operating at 72 MHz (8-leg birdcage, 62 mm diameter, 15 W power). The entire system was inserted in a B_0-cage capable of local earth's field cancelation replaced by a vertical B_0-field of 206 μT. Details on the hardware were demonstrated by Boudries *et al.*, 2023.[24] The system could operate in two distinct modes: either with a Zeeman pre-polarization step of 2 seconds

at 20 mT prior to conventional MRI acquisition at 206 µT (8.77 MHz proton frequency), or with Overhauser enhancement with a constant EPR irradiation at 71.6 MHz throughout proton MRI acquisition at 206 µT.

The MRI sequences used are as follows:

– Zeeman pre-polarization: 2D spin echo (TE/TR: 85/2230 ms), no slice selection, field-of-view: 72 × 72 mm, resolution = 1.1 × 1.1 mm, acquisition time: 270 seconds, and 4 averages.

– OMRI: 2D balanced steady-state free-precession (TE/TR: 67/155 ms), no slice selection, field-of-view: 72 × 72 mm, resolution = 1.1 × 1.1 mm, acquisition time: 30 seconds, and 4 averages. In kinetics experiments, this sequence was repeated every 6 minutes.

Author contributions

Conceptualization: G. C. S., T. E.; funding acquisition: G. C. S., T. E., F. J. M., Ma. P., Me. P., P. E.; resources: G. C. S., T. E., F. J. M., M. P., M. P., P. E., S. R., A. D.; methodology: E. S., R. S., N. M. J., B. D., P. T. J; sample preparation and data acquisition: E. S., R. S., N. M. J., B. D., P. T. J.; data analysis: E. S., R. S., B. D.; data interpretation: E. S., R. S., B. D., Me. P.; visualization: G. C. S., T. E.; supervision: G. C. S., T. E.; writing – original draft: E. S., R. S., G. C. S., T. E. Ma. P.; writing – review and editing: all authors.

Data availability

The data supporting this article have been included as part of the ESI.†

Conflicts of interest

There are no conflicts of interest to declare.

Acknowledgements

References

1 R. H. Wijdeven, J. Neefjes and H. Ovaa, *Trends Cell Biol.*, 2014, **24**, 751–760.

2 C. Yang, Q. Wang and W. Ding, *RSC Adv.*, 2019, **9**, 25285–25302.

3 R. Yan and D. Ye, *Sci. Bull.*, 2016, **61**, 1672–1679.

4 Q. Zhang, T. Liu, J. Ding, N. Zhou, Z. Yu, Y. Ren, X. Qin, P. Du, Z. Yang and H. Zhu, *Mol. Pharm.*, 2022, **19**, 4149–4156.

5 W. Lee, G. Il An, H. Park, S. Sarkar, Y. S. Ha, P. T. Huynh, A. Bhise, N. Bhatt, H. Ahn, D. N. Pandya, J. Y. Kim, S. Kim, E. Jun, S. C. Kim, K. C. Lee and J. Yoo, *ACS Nano*, 2021, **15**, 17348–17360.

6 T. Lindner, A. Altmann, S. Krämer, C. Kleist, A. Loktev, C. Kratochwil, F. Giesel, W. Mier, F. Marme, J. Debus and U. Haberkorn, *J. Nucl. Med.*, 2020, **61**, 1507–1513.

7 I. Daryaei and M. D. Pagel, *Res. Rep. Nucl. Med.*, 2015, **5**, 19–32.

8 D. V. Hingorani, B. Yoo, A. S. Bernstein and M. D. Pagel, *Chem. – Eur. J.*, 2014, **20**, 9840–9850.

9 M. Sarracanie and N. Salameh, *Front. Phys.*, 2020, **8**, DOI: **10.3389/fphy.2020.00172**.

10 M. E. Halse, A. Coy, R. Dykstra, C. Eccles, M. Hunter, R. Ward and P. T. Callaghan, *J. Magn. Reson.*, 2006, **182**, 75–83.

11 L. L. Wald, P. C. McDaniel, T. Witzel, J. P. Stockmann and C. Z. Cooley, *J. Magn. Reson. Imaging*, 2020, **52**, 686–696.

12 A. Mohoric, G. Planinsic, M. Kos, A. Duh and J. Stepisnik, *Instrum. Sci. Technol.*, 2004, **32**, 655–667.

13 A. Abragam and M. Goldman, *Rep. Prog. Phys.*, 1978, **41**, 395.

14 D. J. Lurie, D. M. Bussell, L. H. Bell and J. R. Mallard, *J. Magn. Reson. (1969-1992)*, 1988, **76**, 366–370.

15 D. Grucker, *Magn. Reson. Med.*, 1990, **14**, 140–147.

16 P. Mellet, P. Massot, G. Madelin, S. R. A. Marque, E. Harte, J.-M. Franconi and E. Thiaudière, *PLoS One*, 2009, **4**, e5244.

17 G. Audran, L. Bosco, P. Brémond, J.-M. Franconi, N. Koonjoo, S. R. A. Marque, P. Massot, P. Mellet, E. Parzy and E. Thiaudière, *Angew. Chem., Int. Ed.*, 2015, **54**, 13379–13384.

18 N. Jugniot, I. Duttagupta, A. Rivot, P. Massot, C. Cardiet, A. Pizzoccaro, M. Jean, N. Vanthuyne, J.-M. Franconi, P. Voisin, G. Devouassoux, E. Parzy, E. Thiaudiere, S. R. A. Marque, A. Bentaher, G. Audran and P. Mellet, *Free Radical Biol. Med.*, 2018, **126**, 101–112.

19 D. Alberti, E. Thiaudiere, E. Parzy, S. Elkhanoufi, S. Rakhshan, R. Stefania, P. Massot, P. Mellet, S. Aime and S. Geninatti Crich, *Sci. Rep.*, 2023, **13**, 13725.

20 N. Koonjoo, E. Parzy, P. Massot, M. Lepetit-Coiffé, S. R. A. Marque, J.-M. Franconi, E. Thiaudière and P. Mellet, *Contrast Media Mol. Imaging*, 2014, **9**, 363–371.

21 A. Rivot, N. Jugniot, S. Jacoutot, N. Vanthuyne, P. Massot, P. Mellet, S. R. A. Marque, G. Audran, P. Voisin, M. Delles, G. Devouassoux, E. Thiaudière, A. Bentaher and E. Parzy, *ACS Omega*, 2021, **6**, 15012–15016.

22 T. Guiberteau and D. Grucker, *Phys. Med. Biol.*, 1998, **43**, 1887.

23 M. E. Halse and P. T. Callaghan, *J. Magn. Reson.*, 2008, **195**, 162–168.

24 D. Boudries, P. Massot, E. Parzy, S. Seren, P. Mellet, J.-M. Franconi, S. Miraux, E. Bezançon, S. R. A. Marque, G. Audran, M. Muetzel, S. Wintzheimer, F. Fidler and E. Thiaudiere, *J. Magn. Reson.*, 2023, **348**, 107383.

25 E. Parzy, D. Boudries, S. Jacoutot, M. Albalat, N. Vanthuyne, J.-M. Franconi, P. Mellet, E. Thiaudière, G. Audran, S. R. A. Marque and P. Massot, *J. Magn. Reson.*, 2021, **333**, 107095.

10932 | *J. Mater. Chem. B*, 2024, **12**, 10923–10933

This journal is © The Royal Society of Chemistry 2024

26 S. Elkhanoufi, R. Stefania, D. Alberti, S. Baroni, S. Aime and S. Geninatti Crich, *Chem. – Eur. J.*, 2022, **28**, e202104563.

27 R. Kumari, M. M. Majumder, J. Lievonen, R. Silvennoinen, P. Anttila, N. N. Nupponen, F. Lehmann and C. A. Heckman, *Br. J. Cancer*, 2021, **124**, 1428–1436.

28 T. Fukami and T. Yokoi, *Drug Metab. Pharmacokinet.*, 2012, **27**, 466–477.

29 R. A. Kohnz, M. M. Mulvihill, J. W. Chang, K.-L. Hsu, A. Sorrentino, B. F. Cravatt, S. Bandyopadhyay, A. Goga and D. K. Nomura, *ACS Chem. Biol.*, 2015, **10**, 1624–1630.

30 K. Na, M. Kim, C.-Y. Kim, J.-S. Lim, J.-Y. Cho, H. Shin, H. J. Lee, B. J. Kang, D. H. Han, H. Kim, J.-H. Baik, M. Swiatek-de Lange, J. Karl and Y.-K. Paik, *J. Proteome Res.*, 2020, **19**, 4867–4883.

31 J. Liu, B. Yao, L. Gao, Y. Zhang, S. Huang and X. Wang, *Biochem. Pharmacol.*, 2022, **205**, 115250.

32 G. Xu, W. Zhang, M. K. Ma and H. L. McLeod, *Clin. Cancer Res.*, 2002, **8**, 2605–2611.

33 I. K. Mkam Tsengam, M. Omarova, E. G. Kelley, A. McCormick, G. D. Bothun, S. R. Raghavan and V. T. John, *J. Phys. Chem. B*, 2022, **126**, 2208–2216.

34 D. Wang, L. Zou, Q. Jin, J. Hou, G. Ge and L. Yang, *Acta Pharm. Sin. B*, 2018, **8**, 699–712.

35 S. J. Park, H. W. Lee, H.-R. Kim, C. Kang and H. M. Kim, *Chem. Sci.*, 2016, **7**, 3703–3709.

36 H. J. Braddick, W. J. Tipping, L. T. Wilson, H. S. Jaconelli, E. K. Grant, K. Faulds, D. Graham and N. C. O. Tomkinson, *Anal. Chem.*, 2023, **95**, 5369–5376.

37 G. De Simone, A. di Masi and P. Ascenzi, *Int. J. Mol. Sci.*, 2021, **22**, 10086.

38 P. Ascenzi, L. Leboffe, A. di Masi, V. Trezza, G. Fanali, M. Gioia, M. Coletta and M. Fasano, *PLoS One*, 2015, **10**, e0120603.

39 P. Ascenzi, M. Gioia, G. Fanali, M. Coletta and M. Fasano, *Biochem. Biophys. Res. Commun.*, 2012, **424**, 451–455.

40 S. B. Tove, *Biochim. Biophys. Acta*, 1962, **57**, 230–235.

41 C. S. Johnston, C. G. Meyer and J. C. Srilakshmi, *Am. J. Clin. Nutr.*, 1993, **58**, 103–105.

42 X. Zhuang, C. Xiao, K. Oyaizu, N. Chikushi, X. Chen and H. Nishide, *J. Polym. Sci., Part A: Polym. Chem.*, 2010, **48**, 5404–5410.

43 J. Fuchs, N. Groth, T. Herrling and G. Zimmer, *Free Radical Biol. Med.*, 1997, **22**, 967–976.

44 J. Du, J. J. Cullen and G. R. Buettner, *Biochim. Biophys. Acta, Rev. Cancer*, 2012, **1826**, 443–457.

45 M. Capello, M. Lee, H. Wang, I. Babel, M. H. Katz, J. B. Fleming, A. Maitra, H. Wang, W. Tian, A. Taguchi and S. M. Hanash, *JNCI, J. Natl. Cancer Inst.*, 2015, **107**, djv132.

46 K. Kailass, O. Sadovski, M. Capello, Y. Kang, J. B. Fleming, S. M. Hanash and A. A. Beharry, *Chem. Sci.*, 2019, **10**, 8428–8437.

47 Y. Wen, N. Jing, M. Zhang, F. Huo, Z. Li and C. Yin, *Adv. Sci.*, 2023, **10**, 2206681.

48 K. Na, S.-K. Jeong, M. J. Lee, S. Y. Cho, S. A. Kim, M.-J. Lee, S. Y. Song, H. Kim, K. S. Kim, H. W. Lee and Y.-K. Paik, *Int. J. Cancer*, 2013, **133**, 408–415.

49 N. Qiu, X. Liu, Y. Zhong, Z. Zhou, Y. Piao, L. Miao, Q. Zhang, J. Tang, L. Huang and Y. Shen, *Adv. Mater.*, 2016, **28**, 10613–10622.

50 W. Duan, S. Ji, Y. Guan, X. Mu, S. Fang, Y. Lu, X. Zhou, J. Sun and Z. Li, *Biomacromolecules*, 2020, **21**, 5093–5103.

51 P. Breeuwer, J. L. Drocourt, N. Bunschoten, M. H. Zwietering, F. M. Rombouts and T. Abee, *Appl. Environ. Microbiol.*, 1995, **61**, 1614–1619.

52 D. Hoefel, W. L. Grooby, P. T. Monis, S. Andrews and C. P. Saint, *J. Microbiol. Methods*, 2003, **52**, 379–388.

53 J. Lamego, P. Ferreira, M. Alves, A. Matias and A. L. Simplício, *Mol. Cell. Probes*, 2015, **29**, 215–222.

54 S. Wang, M. Xu, X. Li, X. Su, X. Xiao, A. Keating and R. C. Zhao, *J. Hematol. Oncol.*, 2018, **11**, 82.

55 J. Conde-Vancells, E. Gonzalez, S. C. Lu, J. M. Mato and J. M. Falcon-Perez, *Expert Opin. Drug Metab. Toxicol.*, 2010, **6**, 543–554.

This journal is © The Royal Society of Chemistry 2024

J. Mater. Chem. B, 2024, **12**, 10923–10933 | **10933**